Electronic band structures and native point defects of ultrafine ZnO nanocrystals

Electronic Band Structures and Native Point Defects of Ultrafine ZnO Nanocrystals

Yu-Jia Zeng,[*,†,‡] *Koen Schouteden,*[‡] *Mozhgan N Amini,*[#] *Shuang-Chen Ruan,*[†] *Yang-Fan Lu,*[§] *Zhi-Zhen Ye,*[§] *Bart Partoens,*[#] *Dirk Lamoen,*[#] *and Chris Van Haesendonck*[*,‡]

[†] Shenzhen Key Laboratory of Laser Engineering, College of Optoelectronic Engineering, Shenzhen University, Shenzhen, 518060, P. R. China

[‡] Solid State Physics and Magnetism Section, KU Leuven, Celestijnenlaan 200 D, BE-3001 Leuven, Belgium

[#] CMT & EMAT, Department of Physics, University of Antwerp, Groenenborgerlaan 171, BE-2020 Antwerp, Belgium

[§] State Key Laboratory of Silicon Materials, Department of Materials Science and Engineering, Zhejiang University, Hangzhou 310027, P. R. China

KEYWORDS nanocrystals, scanning tunneling spectroscopy, DFT calculations, zinc oxide, defects.

ABSTRACT Ultrafine ZnO nanocrystals with a thickness down to 0.25 nm are grown by a metalorganic chemical vapor deposition method. Electronic band structures and native point defects of ZnO nanocrystals are studied by a combination of scanning tunneling microscopy/spectroscopy and first-principles density functional theory calculations. Below a critical thickness of about 1 nm ZnO adopts a graphitic-like structure and exhibits a wide band gap similar to its wurtzite counterpart. The hexagonal wurtzite structure, with a well-developed band gap evident from scanning tunneling spectroscopy, is established for a thickness starting from about 1.4 nm. With further increase of the thickness to 2 nm, $V_O - V_{Zn}$ defect pairs are easily produced in ZnO nanocrystals due to the self-compensation effect in highly doped semiconductors.

INTRODUCTION

Semiconductor nanocrystals (NCs) or quantum dots are a class of nanomaterials that bridge the gap between the atomic limit and the bulk solid state, with significant potential for the next-generation nanoelectronics and optoelectronics.[1-4] Among various semiconductor materials ZnO is of particular interest. Its excellent properties, including a direct band gap of 3.37 eV at room temperature, a large exciton binding energy of 60 meV, the availability of high-quality bulk crystals, and a high electron mobility and high thermal conductivity, have stimulated worldwide interest in its bulk and thin-film forms[5-7] as well as in one-dimensional ZnO nanowires.[8-10] On the other hand, considerable research efforts have also been devoted to ZnO NCs.[11-14] In spite of the rapid developments from three dimensions (3D) down to zero dimension (0D), full understanding of the electronic properties of ZnO material remains a major challenge to date. Even the cause of the commonly observed unintentional n-type conductivity in ZnO is still under debate,[6] not to mention the difficulty of reliable p-type doping due to the asymmetric doping limitations.[15,16] Therefore more detailed investigations on ZnO are obviously required to unravel its intrinsic electronic properties.

In contrast to measuring techniques that provide ensemble averaged information, scanning tunneling microscopy (STM) combined with scanning tunneling spectroscopy (STS) allows for the local investigation of the morphology as well as the electronic structure of individual semiconductor NCs with high spatial and energy resolution. STM/STS has already been applied to various semiconductor NCs to study their electronic properties, including InAs,[17,18] CdSe,[19] PdSe,[20] and PdSe/PdS.[21] However, STM/STS investigations of ZnO NCs are very scarce.[22] On the other hand, most of the reported STS studies of ZnO bulk and thin-film forms turn out to be controversial.[23-28] The observed tunneling current gaps vary from zero up to above 3 eV, which,

to some extent, reflects the complicated conductivity in ZnO materials.[6] In this study, we investigate the electronic band structures and point defects in ZnO NCs with a thickness ranging from about 0.25 nm up to a few nanometers. Detailed STM/STS measurements, in combination with first-principles density functional theory (DFT) calculations, reveal that ZnO with a thickness of 0.25 nm adopts a hexagonal graphitic-like structure in which the Zn and O atoms are coplanar. A hexagonal wurtzite structure is established in ZnO NCs with a thickness around 1.4 nm. With further increase of the thickness (2 − 3 nm), native point defects start to appear in the ZnO NCs, probably in the form of oxygen vacancy – zinc vacancy pairs (V_O−V_{Zn}). These novel findings considerably improve our understanding of the growth of and defect formation in ZnO material. In particular, 2D hexagonal graphitic-like ZnO is expected to have unique electronic properties like other 2D materials, such as graphene and MoS_2, which are of fundamental importance to future ZnO based device development.

RESULTS AND DISCUSSION

ZnO NCs were grown by a low-pressure metalorganic chemical vapor deposition (MOCVD) method[29] on Au (111) substrates. In **Figure 1** we present a large area STM topography image as well as the corresponding 3D view of the ZnO NCs. It is evident from these images that ZnO NCs have different thicknesses ranging from a few angstroms up to more than 2 nm. We will demonstrate below that ZnO NCs with different thicknesses have very distinct electronic properties. In **Figure 2a** we present an STM topography image of the thinner ZnO NCs. The herringbone reconstruction is resolved on the surrounding atomically flat Au surface,[30] illustrating the cleanliness of the ex-situ growth process and the reliability of the annealing steps (see the Experimental Section). There exist two different types of ZnO NCs. The height profile along the blue straight line in Figure 2a gives two typical apparent height values of about 0.25

nm and 0.90 nm (Figure 2b). The 0.25 nm ZnO appears as a percolating two-dimensional layer, while the 0.90 nm ZnO rather appears as a collection of closely spaced individual NCs. In Figure 2c we compare the voltage V dependence of the tunneling current I for these two types of ZnO NCs as well as for the Au substrate, which are all recorded at the same tunneling settings. In contrast to the metallic Au substrate, both ZnO NCs reveal a clear suppression of the tunnelling current around the Fermi level which is located at 0 V. The $I(V)$ spectra of the NCs often are asymmetric with respect to the Fermi level.[22] The 0.90 nm ZnO shows a well-developed electron band gap of about 5.2 eV indicated by the small black arrows. On the other hand, the 0.25 nm ZnO shows a slow increase of the tunnelling current around the Fermi level. We conclude that the two types of ZnO NCs have different electronic properties, which are accompanied by significantly different STM topographies.

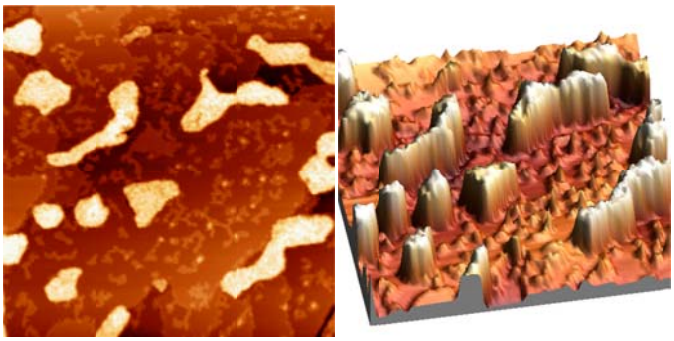

Figure 1. 300 × 300 nm^2 STM topography image and the corresponding 3D view of ZnO NCs (color height scale 2.3 nm, I = 0.4 nA, V = 3 V).

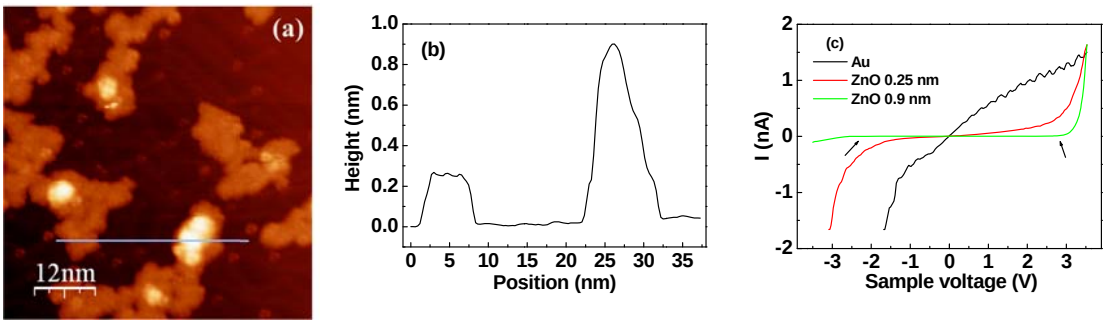

Figure 2. (a) 60 × 60 nm^2 STM topography image of ZnO NCs on Au (111) (color height scale 0.95 nm, I = 3 nA, V = 3.25 V). (b) Height profile along the blue straight line in Figure 1(a). (c) $I-V$ spectra of ZnO NCs with different thicknesses and of the Au substrate. The arrows indicate the edge of the band gap.

ZnO typically exhibits a hexagonal wurtzite structure in its bulk form as well as in nanomaterials, where Zn and O atoms are arranged in a tetrahedral configuration. However, a novel graphitic-like structure has been theoretically proposed for wurtzite material in order to stabilize its polar surface when the thickness is reduced down to a few atomic layers.[31] A graphitic-like structure in which the Zn and O atoms are coplanar has been experimentally observed in ZnO grown on Ag (111),[32] Pd (111)[33] and Au (111)[34] substrates.

We performed first-principles DFT calculations on both wurtzite and graphitic-like ZnO slabs. By relaxing each structure, we are able to identify the thermodynamically more favorable structures of ZnO for different thicknesses. **Table 1** summarizes the favorable structures at different thicknesses and the corresponding electron band gaps calculated with different hybrid exchange-correlation functionals. ZnO prefers the graphitic-like structure for thicknesses of 0.23, 0.70 and 0.98 nm. The wurtzite structure becomes thermodynamically more favorable when the thickness increases to 1.37 nm. The calculations can be linked to our experimental STM/STS

results. We note that STM typically underestimates the actual height of ZnO NCs due to the reduced conductivity of the oxide as compared to the metallic Au substrates.[34,35] The 0.90 nm ZnO observed in Figure 2 therefore likely corresponds to the thickness of 1.37 nm indicated in Table 1 (or to an even larger thickness). In Figure 2(c) the 0.90 nm ZnO reveals a gap of about 5.2 eV, which is in agreement with the calculations on wurtzite ZnO (1.37 nm) using the PBE0 functional (4.8 eV). Here we also demonstrate that in this thickness regime the PBE0 (4.80 eV) provides a better estimate of the electron band gap than the HSE functional (3.74 eV, see Table 1). Concerning the 0.25 nm ZnO, our calculations point out that ZnO adopts a graphitic-like structure rather than a wurtzite one in this thickness regime. On the other hand, our calculations also point to a wide band gap of 4.98 − 5.30 eV for graphitic-like ZnO using the PBE0 functional, which is larger than the gap value inferred from Figure 2c. We assume that the ZnO-Au interface local density of states (LDOS) starts to dominate the STS when the thickness of ZnO decreases down to a few atomic layers, which is similar to the case of NaCl on a Cu substrate.[35] Therefore we cannot make a reliable estimate of the band gap based on STS for the thinnest ZnO. Note that our results together with previous studies show that graphitic-like ZnO can be grown not only on Au (111) substrates[34] but also on Ag (111)[32] as well as Pd (111)[33] substrate, implying an universal mechanism to stabilize the polar surface.[31]

Table 1. DFT results for the thermodynamically favorable structures of ZnO for different thicknesses and the corresponding electron band gaps calculated with different hybrid exchange-correlation functionals.

Thickness [nm]	Favorable structure	E_g (HSE)	E_g (PBE0)
0.23	graphitic-like	4.23	5.30
0.70	graphitic-like	4.13	5.15

0.98	graphitic-like	3.89	4.98
1.37	wurtzite	3.74	4.80

Now we move to the thicker ZnO NCs with a thickness around 2.5 nm. In **Figure 3a** we present an STM topography image of an aggregate of multiple ZnO NCs. STS d*I*/d*V* spectra recorded at different locations are presented in Figure 3b. The STS spectra indicate the presence of a band gap around 3 eV, which is in good agreement with that of bulk ZnO. In addition, the spectra also reveal energy states inside the band gap on both sides of the Fermi level, which are not observed in the thinner ZnO NCs with thickness below 1 nm (Figure 2). In **Figure S1** we present more results for ZnO NCs with varying thickness (from about 0.8 nm up to 2 nm). Consistent with the above-mentioned observations in Figure 2 and Figure 3, a thinner area tends to have a larger band gap, while a thicker area typically exhibits a smaller band gap with energy states appearing inside the gap. This can be visualized more clearly in a *dI/dV*(V) grid measurement. In **Figure 4** we present *dI/dV*(V) maps at different selected voltages. For each voltage the bright area indicates a larger *dI/dV* value, i.e., a larger LDOS. It can be seen that on the ZnO NCs the LDOS becomes completely suppressed at zero voltage (the Fermi level), which results from the presence of a band gap of the semiconductor. At certain voltages (± 0.5 V and ±1 V), there appears a non-zero LDOS on some areas of the NCs, i.e., on the thicker NCs regions (~ 2 nm). The appearance of a non-zero LDOS, in particular at low voltages around ± 0.5 V, can be linked to the presence of energy states inside the band gap of the ZnO NCs. On the other hand, the LDOS remains suppressed even at a voltage of − 2 V for the thinner areas (0.8 nm), indicating a large band gap without energy states inside the gap. Systematic examination of our STS data reveals that the energy states inside the band gap of ZnO, if present, always appear simultaneously on both sides of the Fermi level (Figure 3b). In other words, we hardly observe a

donor-like state or an acceptor-like state existing alone as these states tend to form pairs. We summarize these observations in **Figure S2** in a schematic way.

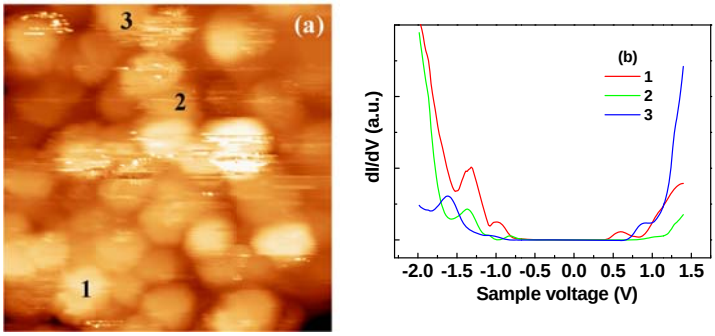

Figure 3. (a) 20 × 20 nm^2 STM topography image of ZnO NCs with thickness up to 2.5 nm (I = 1 nA, V = 1.6 V). (b) STS on the ZnO NCs at the different locations indicated in (a).

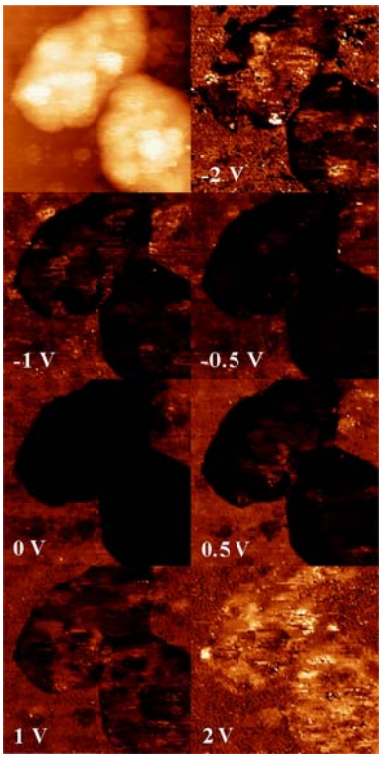

Figure 4. 42 × 42 nm^2 STM topography image (upper left, color height scale 2.4 nm, I = 2.5 nA, V = 2 V) and corresponding local density of states maps of ZnO NCs recorded at different voltages using constant height mode.

Our ZnO NCs are nominally undoped semiconductors. The most probable candidates for the observed donor and acceptor states are native point defects in ZnO. The fact that the energy states are only present in the thicker regions (more than 2 nm) indicates that the probability for the appearance of native point defects increases with increasing ZnO thickness (or volume), which seems very reasonable. However, the question remains why the defects always appear as donor-acceptor pairs. It has been reported that the addition of 1.4×10^{21} cm^{-3} Ga donors in ZnO causes the lattice to spontaneously form 1.7×10^{20} cm^{-3} V_{Zn} acceptors,[36] which is explained by the so-called self-compensation effect that tends to occur in highly doped semiconductors, i.e., the tendency of a crystal to lower its energy by forming point defects to counter the effects of doping. Assuming one ZnO NC contains 1000 Zn (or O) atoms, only one point defect already results in a concentration up to 4×10^{19} cm^{-3}. Therefore, the here observed formation of defect pairs can be ascribed to the above mentioned self-compensation effect in our ZnO NCs, which appear to be highly doped by native point defects.

To clarify the origin of the energy states inside the band gap of ZnO, we perform first-principles DFT calculations with the hybrid HSE06 functional. Among all the native point defects, V_O (donor) and V_{Zn} (acceptor) defects have the lowest formation energy.[6] However, their combination has not been studied in detail. Here we considered three different configurations (P_1, P_2 or P_3) for a V_O–V_{Zn} pair in the bulk ZnO supercell consisting of 108 atoms (**Figure S3**). Comparing the total energy after relaxation, we find the most stable configuration (P_1) for the defect pair in ZnO. We then calculate the formation energy as a function of the Fermi level

position for the V_O–V_{Zn} pairs, as illustrated in **Figure 5**. The kinks in the curves indicate transitions between different charge states. Note that in the neutral state for a donor-acceptor pair, the electrons of the donor level are transferred to the acceptor level, resulting in an empty donor level and an occupied acceptor level. Therefore, the positive and negative charge state of a donor-acceptor pair corresponds to the acceptor level and the donor level, respectively, which is opposite to the case of a single donor and a single acceptor level. In Figure 5 one can see that there exist 1+ and 2+ charge states close to the valence band maximum, which both stem from the V_{Zn} acceptor level. On the other hand, only a 2− charge state is allowed close to the conduction band minimum, which stems from the V_O donor level. Our calculations reveal a good candidate to explain the experimental observations. In the three curves in Figure 3(b) we do observe two peaks in the negative voltage range, which can be attributed to the occupied V_{Zn} in the $V_O - V_{Zn}$ pair. The single feature in the positive voltage range (peak in the red and blue curve; a bump in the green curve) can be ascribed to the empty V_O in the V_O–V_{Zn} pair. The variation in the peak position is believed to be the result of the different tip-induced band bending due to the different shapes of the NCs.

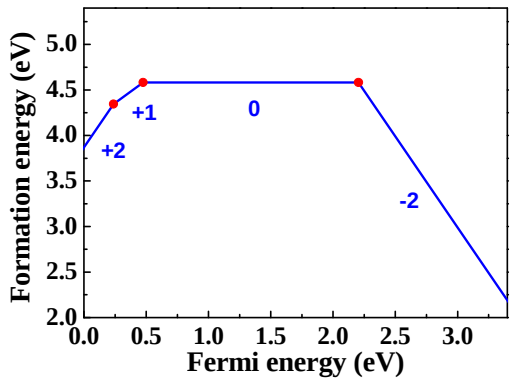

Figure 5. Formation energy as a function of Fermi level position for a V_O–V_{Zn} pair. The zero of Fermi level corresponds to the valence band maximum. Only segments corresponding to the lowest energy charge states are shown.

Finally we want to stress that the presence of V_O–V_{Zn} pairs is universal in the thicker ZnO NCs above 2 nm. In fact we hardly find regions without the defect pairs, indicating an important compensation effect in the ZnO material. We suggest that such donor-acceptor pairs are also present in bulk p-type doped ZnO. Due to the relatively deep acceptor level in ZnO,[15,16] a high concentration of acceptors is required to achieve a sufficient hole concentration. On the other hand, a high concentration of acceptors will result in the formation of donor-acceptor pairs due to the self-compensation effect in highly doped ZnO. In the case of p-type doping, such donor-acceptor pairs consist of an oxygen vacancy and an extrinsic p-type dopant, for example a V_O–N_O pair, which might be one of the important causes for the bottleneck in p-type doping of ZnO.

CONCLUSION

In conclusion, we investigated the electronic band structures and native point defects of ultrafine ZnO nanocrystals by a combination of scanning tunneling microscopy/spectroscopy and first-principles density functional theory calculations. We find that below a critical thickness of about 1 nm ZnO adopts a graphitic-like structure. The hexagonal wurtzite structure is established in ZnO NCs with a thickness starting from about 1.4 nm. With further increase of the thickness to 2 nm, V_O–V_{Zn} defect pairs are easily produced in ZnO NCs due to the self-compensation effect in highly doped semiconductors. Our experimental and theoretical results shed light on the remarkable structure as well as on point defects formation in ZnO and may help to understand

the long-time unsettled p-type doping issues. Graphitic-like ZnO may combine the unique electronic properties associated with 2D materials and the excellent optical properties of wurtzite ZnO.

METHODS

Experimental ZnO NCs were grown by a catalyst-free, low-pressure MOCVD method. Diethylzinc (DEZn) and O_2 were used as the zinc source and oxygen source, respectively. N_2 was used as the carrier gas. The growth temperature was 450 ºC. The chamber pressure was maintained at 2 Pa during the growth of the ZnO. Clean atomically flat Au (111) films[37] were used as the substrates. By carefully controlling the growth time as well as the source gas flow, we were able to deposit ultrafine ZnO NCs on the Au substrate, with a thickness ranging from a few angstroms up to more than 2 nm. An annealing treatment at 450 ºC in vacuum was always performed prior to ZnO deposition and prior to STM/STS measurements in order to remove the adsorbed contaminants (e.g., water) due to exposure of the sample to ambient conditions. STM/STS measurements were performed with an ultra-high vacuum (base pressure in the 10^{-11} mbar range) STM setup (Omicron Nanotechnology) at 4.5 K using mechanically cut PtIr (10 % Ir) tips. Spectra of the tunneling current I and of the tunneling conductance dI/dV versus the tunneling voltage V (V is the voltage applied to the sample, while the STM tip is virtually grounded) are acquired with open feedback loop. dI/dV spectra, which directly reflect the LDOS, are obtained by lock-in detection at a modulation frequency of 840 Hz and with a sample voltage modulation amplitude in the 10 to 50 mV range. $I(V)$ spectra can also be acquired in a grid of typically 200×200 points. From such grids, spatial dI/dV maps can be obtained at selected voltages V by numerical differentiation. Image processing is performed by Nanotec WSxM.[38]

Computational Details First-principles total-energy calculations were performed using DFT with the screened hybrid functional of Heyd, Scuseria, and Ernzerhof (HSE06)[39] and the Perdew, Burke and Ernzerhof (PBE0) hybrid functional,[40,41] as implemented in the Vienna ab initio simulation package.[42,43] The accuracy of the semilocal PBE approach was improved by mixing its exchange energy with a fraction of the exact nonlocal Hartree-Fock exchange energy, leading to hybrid functionals such as PBE0. Moreover, the electron-electron interaction was further separated into short- and long-range parts. Considering only short-range Fock exchange resulted in a decrease in computational time while preserving the accuracy of the calculations such as in HSE06. Using these methods substantially improved the band gaps and electronic properties. We used the HSE06 functional in all our calculations, except for the determination of the band gap value of different ZnO layers, for which we applied PBE0 as well. It has been found that for small-gap semiconductors, HSE results in better band gap values compared to the PBE0, while the latter works better for large-gap semiconductors.[44] We used an optimized 37.5% Hartree-Fock exchange mixing in the HSE06 functional. This mixing correctly reproduced the experimental value of the band gap in ZnO.[45] Electron-ion interactions were treated using projector augmented wave potentials.[46,47] The Zn ($4s^2 3d^{10}$) and O ($2s^2 2p^6$) electrons were treated as valence electrons. The electron wave functions were expanded with a plane wave basis set up to a cutoff energy of 400 eV, and the Brillouin zone was sampled with a k-point grid of 2×2×2 in case of bulk calculations and 4×4×1 for slab calculations. Note that the convergence with respect to self-consistent iterations was assumed when the total energy difference between cycles was less than 10^{-4} eV and the geometry relaxation for different charge states continued until the transition level position differences were less than 10 meV. For the defect pair calculations, three different configurations were considered for a V_O–V_{Zn} pair in the bulk ZnO supercell consisting

of 108 atoms. Comparing the total energy after relaxation, we find the most stable configuration for the defect pair in ZnO.

ASSOCIATED CONTENT

Supporting Information. STM topography image and $I-V$ curves; Schematic overview of electronic band structures; different configurations of V_O-V_{Zn} pairs. This material is available free of charge via the Internet at http://pubs.acs.org.

AUTHOR INFORMATION

Corresponding Author

E-mail: yjzeng@szu.edu.cn, chris.vanhaesendonck@fys.kuleuven.be

ACKNOWLEDGMENT

This work was supported at KU Leuven by the Research Foundation − Flanders (FWO, Belgium) as well as by the Flemish Concerted Research Action (BOF KU Leuven, GOA/14/007) research program. The calculations were carried out using the HPC infrastructure at the University of Antwerp (CalcUA), a division of the Flemish Supercomputer Center VSC, supported financially by the Hercules foundation and the Flemish Government (EWI Department). The work at Shenzhen University was supported by National Natural Science Foundation of China under Grant No. 61275144. The work at Zhejiang University was supported by the National Natural Science Foundation of China under Grant No. 51202217.

REFERENCES

(1) Alivisatos, A. P. Semiconductor Clusters, Nanocrystals, and Quantum Dots. *Science* **1996**, *271*, 933-937.

(2) Yoffe, A. D. Semiconductor Quantum Dots and Related Systems: Electronic, Optical, Luminescence and Related Properties of Low Dimensional Systems. *Adv. Phys.* **2001**, *50*, 1-208.

(3) Burda, C.; Chen, X. B.; Narayanan, R.; El-Sayed, M. A. Chemistry and Properties of Nanocrystals of Different Shapes. *Chem. Rev*. **2005**, *105*, 1025-1102.

(4) Smith, A. M.; Nie, S. M. Semiconductor Nanocrystals: Structure, Properties, and Band Gap Engineering. *Acc. Chem. Res.* **2010**, *43*, 190-200.

(5) Özgür, Ü.; Alivov, Y. I.; Liu, C.; Teke, A.; Reshchikov, M. A.; Doğan, S.; Avrutin, V.; Cho, S. J.; Morkoc, H. A Comprehensive Review of ZnO Materials and Devices. *J. Appl. Phys.* **2005**, *98*, (041301), 1-103.

(6) Janotti, A.; Van de Walle, C. G. Fundamentals of Zinc Oxide as a Semiconductor. *Rep. Prog. Phys.* **2009**, *72*, **(**126501), 1-29.

(7) Klingshirn, C.; Fallert, J.; Zhou, H.; Sartor, J.; Thiele, C.; Maier-Flaig, F.; Schneider, D.; Kalt, H. 65 Years of ZnO Research - Old and Very Recent Results. *Phys. Status Solidi B* **2010**, *247*, 1424-1447.

(8) Pearton, S. J.; Norton, D. P.; Ren, F. The Promise and Perils of Wide-Bandgap Semiconductor Nanowires for Sensing, Electronic, and Photonic Applications. *Small* **2007**, *3*, 1144-1150.

(9) Wang, Z. L. Splendid One-Dimensional Nanostructures of Zinc Oxide: A New Nanomaterial Family for Nanotechnology. *ACS Nano* **2008**, *2*, 1987-1992.

(10) Zeng, Y. J.; Pereira, L. M. C.; Menghini, M.; Temst, K.; Vantomme, A.; Locquet, J.-P.; Van Haesendonck, C. Tuning Quantum Corrections and Magnetoresistance in ZnO Nanowires by Ion Implantation. *Nano Lett.* **2012**, *12*, 666-672.

(11) Ischenko, V.; Polarz, S.; Grote, D.; Stavarache, V.; Fink, K,; Driess, M. Zinc Oxide Nanoparticles with Defects. *Adv. Funct. Mater*. **2005**, *15*, 1945-1954.

(12) Kahn, M. L.; Monge, M.; Snoeck, E.; Maisonnat, A.; Chaudret, B. Spontaneous Formation of Ordered 2D and 3D Superlattices of ZnO Nanocrystals. *Small* **2005**, *1*, 221-224.

(13) Zeng, Y. J.; Lin, S. S.; Volodin, A.; Lu, Y. F.; Ye, Z. Z.; Van Haesendonck, C. Zero-Dimensional Field Emitter Based on ZnO Quantum Dots. *Appl. Phys. Lett.* **2010**, *97*, (143102), 1-3.

(14) Liu, W. K.; Whitaker, K. M.; Smith, A. L.; Kittilstved, K. R.; Robinson, B. H.; Gamelin, D. R. Room-Temperature Electron Spin Dynamics in Free-Standing ZnO Quantum Dots. *Phys. Rev. Lett.* **2007**, *98*, (186804), 1-4.

(15) Zhang, S. B.; Wei, S.-H.; Zunger, A. Intrinsic N-type versus P-type Doping Asymmetry and the Defect Physics of ZnO. *Phys. Rev. B* **2001**, *63*, (075205), 1-7.

(16) Avrutin, V.; Silversmith, D. J.; Morkoc, H. Doping Asymmetry Problem in ZnO: Current Status and Outlook. *Proc. IEEE*, **2010**, *98*, 1269-1280.

(17) Mocatta, D.; Cohen, G.; Schattner, J.; Millo, O.; Rabani, E.; Banin, U. Heavily Doped Semiconductor Nanocrystal Quantum Dots. *Science* **2011**, *332*, 77-81.

(18) Maltezopoulos, T.; Bolz, A.; Meyer, C.; Heyn, C.; Hansen, W.; Morgenstern, M.; Wiesendanger, R. Wave-Function Mapping of InAs Quantum Dots by Scanning Tunneling Spectroscopy. *Phys. Rev. Lett.* **2003**, *91*, (196804), 1-4.

(19) Jdira, L.; Overgaag, K.; Gerritsen, J.; Vanmaekelbergh, D.; Liljeroth, P.; Speller, S. Scanning Tunnelling Spectroscopy on Arrays of CdSe Quantum Dots: Response of Wave Functions to Local Electric Fields. *Nano Lett.* **2008**, *8*, 4014-4019.

(20) Overgaag, K.; Liljeroth, P.; Grandidier, B.; Vanmaekelbergh, D. Scanning Tunneling Spectroscopy of Individual PbSe Quantum Dots and Molecular Aggregates Stabilized in an Inert Nanocrystal Matrix. *ACS Nano*, **2008**, *2*, 600-606.

(21) Grinbom, G. A.; Saraf, M.; Saguy, C.; Bartnik, A. C.; Wise, F.; Lifshitz, E. Density of States in a Single PbSe/PbS Core-shell Quantum Dot Measured by Scanning Tunneling Spectroscopy. *Phys. Rev. B* **2010**, *81*, (245301), 1-7.

(22) Schouteden, K.; Zeng, Y. J.; Lauwaet, K.; Romero, C. P.; Goris, B.; Bals, S.; Van Tendeloo, G.; Lievens, P.; Van Haesendonck, C. Band Structure Quantization in Nanometer Sized ZnO. *Nanoscale* **2013**, *5*, 3757-3763.

(23) Bonnel, D. A. Scanning Tunneling Microscopy and Spectroscopy of Oxide Surfaces. *Prog. Surf. Sci.* **1998**, *57*, 187-252.

(24) Urbieta, A.; Fernández, P.; Piqueras, J.; Vasco, E.; Zaldo, C. Scanning Tunneling Microscopy Study of the Surface Electrical Properties of ZnO Films Grown by Pulsed Laser Deposition. *Phys. Status Solidi A* **2003**, *195*, 183-188.

(25) Yin, X. L.; Birkner, A.; Hanel, K.; Lober, T.; Kohler, U.; Woll, C. Adsorption of Atomic Hydrogen on ZnO(1010): STM Study. *Phys. Chem. Chem. Phys.* **2006**, *8*, 1477-1481.

(26) Dumont, J.; Hackens, B.; Faniel, S.; Mouthuy, P.-O.; Sporken, R.; Melinte, S. ZnO(0001) Surfaces Probed by Scanning Tunneling Spectroscopy: Evidence for an Inhomogeneous Electronic Structure. *Appl. Phys. Lett.* **2009**, *95*, (132102), 1-3.

(27) Likovich, E. M.; Jaramillo, R. Russell, K. J.; Ramanathan, S.; Narayanamurti, V. Scanning Tunneling Microscope Investigation of Local Density of States in Al-doped ZnO Thin Films. *Phys. Rev. B* **2011**, *83*, (075430), 1-6.

(28) Zheng, H.; Kroger, J.; Berndt, R. Spectroscopy of Single Donors at ZnO(0001) Surfaces. *Phys. Rev. Lett.* **2012**, *108*, (076801), 1-5.

(29) Zeng, Y. J.; Ye, Z. Z.; Liu, F.; Li, D. Y.; Lu, Y. F.; Jaeger, W.; He, H. P.; Zhu, L. P.; Huang, J. Y.; Zhao, B. H. Controllable Growth and Characterization of ZnO MgO Quasi Core-Shell Quantum Dots. *Cryst. Growth Des.* **2009**, *9*, 263-266.

(30) Barth, J. V.; Brune, H.; Ertl, G.; Behm, R. J. Scanning Tunneling Microscopy Observations on the Reconstructed Au(111) Surface: Atomic Structure, Long-range Superstructure, Rotational Domains, and Surface Defects. *Phys. Rev. B* **1990**, *42*, 9307-9318.

(31) Freeman, C. L.; Claeyssens, F.; Allan, N. L.; Harding, J. H. *Graphitic Nanofilms as Precursors to Wurtzite Films: Theory. Phys. Rev. Lett.* **2006**, *96*, (066102), 1-4.

(32) Tusche, C.; Meyerheim, H. L.; Kirschner, J. Observation of Depolarized ZnO(0001) Monolayers: Formation of Unreconstructed Planar Sheets. *Phys. Rev. Lett.* **2007**, *99*, (026102), 1-4.

(33) Weirum, G.; Barcaro, G.; Fortunelli, A.; Weber, F. Schennach, R. Surnev, S.; Netzer, F. P. Growth and Surface Structure of Zinc Oxide Layers on a Pd(111) Surface, *J. Phys. Chem. C* **2010**, *114*, 15432–15439.

(34) Deng, X.; Yao, K.; Sun, K.; Li, W. X.; Lee, J.; Matranga, C. Growth of Single- and Bilayer ZnO on Au(111) and Interaction with Copper. *J. Phys. Chem. C* **2013**, *117*, 11211−11218.

(35) Repp, J.; Meyer, G.; Rieder, K. H. Snell's Law for Surface Electrons: Refraction of an Electron Gas Imaged in Real Space. *Phys. Rev. Lett.* **2004**, *92*, (036803), 1-4.

(36) Look, D. C.; Leedy, K. D.; Vines, L.; Svensson, B. G.; Zubiaga, A.; Tuomisto, F.; Doutt, D. R.; Brillson, L. J. Self-compensation in Semiconductors: The Zn Vacancy in Ga-doped ZnO. *Phys. Rev. B* **2011**, *84*, (115202), 1-6.

(37) Schouteden, K.; Lando, A.; Janssens, E.; Lievens, P.; Van Haesendonck, C. Morphology and Electron Confinement Properties of Co Clusters Deposited on Au(111). *New J. Phys.* **2008**, *10*, (083005), 1-15.

(38) Horcas, I.; Fernandez, R.; Gomez-Rodriguez, J. M.; Colchero, J.; Gomez-Herrero, J.; Baro, A. M. WSXM: A Software for Scanning Probe Microscopy and a Tool for Nanotechnology. *Rev. Sci. Instrum.* **2007**, *78*, (013705), 1-8.

(39) Heyd, J.; Scuseria, G. E.; Ernzerhof, M. Hybrid Functionals Based on a Screened Coulomb Potential. *J. Chem. Phys.* **2003**, *118*, 8207-8215.

(40) Perdew, J. P.; Burke, K.; Ernzerhof, M. Generalized Gradient Approximation Made Simple. *Phys. Rev. Lett.* **1996**, *77*, 3865-3868.

(41) Adamo, C.; Barone, V. Toward Reliable Density Functional Methods without Adjustable Parameters: The PBE0 Model. *J. Chem. Phys.* **1999**, *110,* 6158-6170.

(42) Kresse, G.; Furthmüller, Efficiency of ab-initio Total Energy Calculations for Metals and Semiconductors using a Plane-wave Basis Set. J. *Comput. Mater. Sci.* **1996**, *6*, 15-50.

(43) Kresse, G.; Furthmüller, J. Efficient Iterative Schemes for ab initio Total-Energy Calculations using a Plane-wave Basis Set. *Phys. Rev. B* **1996**, *54*, 11169-11186.

(44) Matsushita, Y. I.; Nakamura, K.; Oshiyama, A. Comparative Study of Hybrid Functionals Applied to Structural and Electronic Properties of Semiconductors and Insulators. *Phys. Rev. B* **2011**, *84,* (075205), 1-13.

(45) Janotti, A.; Van de Walle, C. G. LDA + U and Hybrid Functional Calculations for Defects in ZnO, SnO_2, and TiO_2. *Phys. Status Solidi B* **2011**, *248*, 799-804.

(46) Kresse, G.; Joubert, D. From Ultrasoft Pseudopotentials to the Projector Augmented-wave Method. *Phys. Rev. B* **1999**, *59*, 1758-1775.

(47) Adolph, B.; Furthmüller, J.; Bechstedt, F. Optical Properties of Semiconductors using Projector-augmented Waves. *Phys. Rev. B* **2001**, *63*, (125108), 1-8.

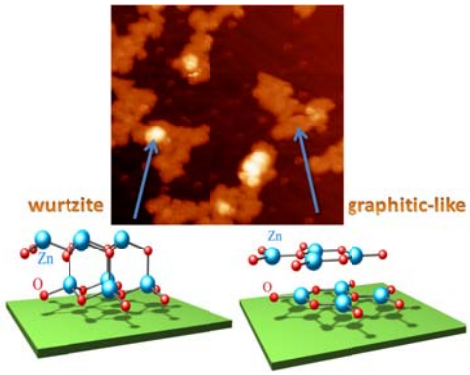

Table of Contents